Hybrid Materials

International Edition: DOI: 10.1002/anie.201509557
German Edition: DOI: 10.1002/ange.201509557

Redox-Active Corannulene Buckybowls in a Crystalline Hybrid Scaffold

*W. Brett Fellows[+], Allison M. Rice[+], Derek E. Williams, Ekaterina A. Dolgopolova, Aaron K. Vannucci, Perry J. Pellechia, Mark D. Smith, Jeanette A. Krause, and Natalia B. Shustova**

Abstract: *A porous crystalline corannulene-containing scaffold, which combines the periodicity, dimensionality, and structural modularity of hybrid frameworks with the intrinsic properties of redox-active π-bowls, has been prepared. Single-crystal and powder X-ray diffraction, ab initio density functional theory computations, gas sorption analysis, fluorescence spectroscopy, and cyclic voltammetry were employed to study the properties of the novel corannulene derivatives and the buckybowl-based hybrid materials. X-ray diffraction studies revealed the preservation of the corannulene bowl inside the prepared rigid matrix, which offers the unique opportunity to extend the scaffold dimensionality through the buckybowl curvature. Merging the inherent properties of hybrid frameworks with the intrinsic properties of π-bowls opens a new avenue for preparing redox-active materials and potentially improving charge transport in the scaffold.*

The bowl-shaped surface of corannulene, $C_{20}H_{10}$, has attracted a lot of attention owing to its intriguing curvature.[1–6] However, only recently a more practical synthetic route[7] rendered $C_{20}H_{10}$ available for comprehensive studies, which has also boosted its utilization in a wide scope of applications.[8–14] For instance, acceptance of four electrons makes corannulene more electron-rich per carbon atom than the commonly used electron acceptor fullerene.[15,16] Moreover, the electron-accepting properties can be tuned through derivatization of the $C_{20}H_{10}$ bowl.[17] Corannulene also possesses a high degree of lithium intercalation, as exemplified by the sandwich-like structure consisting of two corannulene tetraanions with five lithium cations incorporated between them (Scheme 1).[15] Furthermore, the reversible lithium capacity of corannulene-based materials is almost twice as high as that of lithiated graphite,[18] rendering corannulene derivatives promising building blocks for the preparation of anode materials in rechargeable lithium-ion batteries.

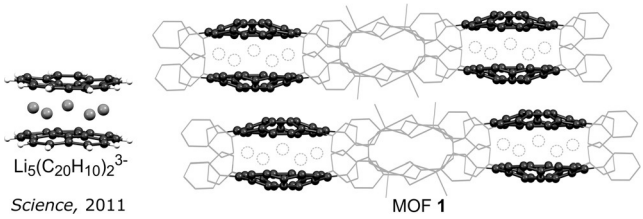

Scheme 1. Left: Corannulene-based sandwich (adapted with permission from Ref. [15]). Right: The prepared crystalline scaffold suitable for potential guest (e.g., alkali metal) incorporation.

Herein, we report the development of a hybrid framework built from novel redox-active corannulene-based ligands. In contrast to previously reported corannulene-containing polymers,[19–23] we have synthesized the first example of a porous crystalline scaffold in which the derivatized buckybowl is covalently linked to metal ions. Coordinative immobilization of the corannulene-based linker inside the metal–organic framework (MOF) preserves the bowl shape, which may offer an extension of scaffold dimensionality through the corannulene curvature. By analogy with the reduced corannulene-based "sandwich",[15,24] the prepared crystalline scaffold can be considered a "baguette", for instance, for alkali-metal intercalation (Scheme 1). Moreover, incorporation of redox-active corannulene-based ligands opens a new avenue to improve MOF charge-transport properties and develop a new family of electrochromic materials. In the presented work, single-crystal and powder X-ray crystallography, spectroscopic studies, gas sorption analysis, and cyclic voltammetry were employed for comprehensive analysis of the prepared corannulene-based scaffold. Therefore, these studies are the first attempt to bridge the structural modularity and porosity of MOFs with the intrinsic properties of π-bowls.

While milligram-scale reactions are typically reported for the preparation of new corannulene derivatives,[25–27] one of the challenges in the development of corannulene-containing MOFs is the synthesis of the corresponding ligand in multigram quantities. The amount of ligand is dictated by the combinatorial approach typically used for MOF self-assembly[28–31] and, more importantly, comprehensive analysis of the prepared materials. Therefore, 1,2,7,8-tetrabromocorannulene, which is accessible on gram scale (Scheme 2),[7] was chosen as a precursor for the preparation of the corannulene-based linker with four carboxylic acids for subsequent metal

[*] Dr. W. B. Fellows,[+] A. M. Rice,[+] D. E. Williams, E. A. Dolgopolova, Prof. Dr. A. K. Vannucci, Dr. P. J. Pellechia, Dr. M. D. Smith, Prof. Dr. N. B. Shustova
Department of Chemistry and Biochemistry
The University of South Carolina
631 Sumter Street, Columbia, SC 29208 (USA)
E-mail: shustova@sc.edu
Dr. J. A. Krause
Department of Chemistry
The University of Cincinnati
Cincinnati, OH 45221 (USA)
[+] These authors contributed equally to this work.

Supporting information for this article is available on the WWW under http://dx.doi.org/10.1002/anie.201509557.

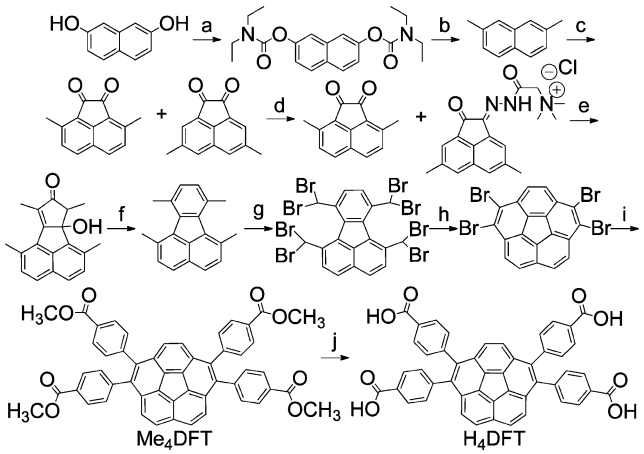

Scheme 2. Synthesis of H_4DFT: a) diethylcarbamoyl chloride, pyridine, 100 °C, 2 d; b) MeMgBr, $NiCl_2(dppp)_2$, Et_2O, 30 °C, 13 h; c) $AlBr_3$, $(COCl)_2$, CH_2Cl_2, −15 °C, 8 h; d) Girard's reagent T, AcOH, 40 °C, 2 h; e) 3-pentanone, KOH, MeOH, 2 h; f) norbornadiene, Ac_2O, 140 °C, 3 d; g) NBS, benzoyl peroxide, CCl_4, *hν*, 77 °C, 5 d; h) NaOH, dioxane/H_2O, 100 °C, 1 h; i) 4-(carboxymethyl)phenylboronic acid, methyl 4-iodobenzoate, K_3PO_4, $Pd(PPh_3)_4$, dioxane, 100 °C, 5 d; j) NaOH, MeOH/THF/H_2O, 80 °C, 3 d; then HCl/water, RT.

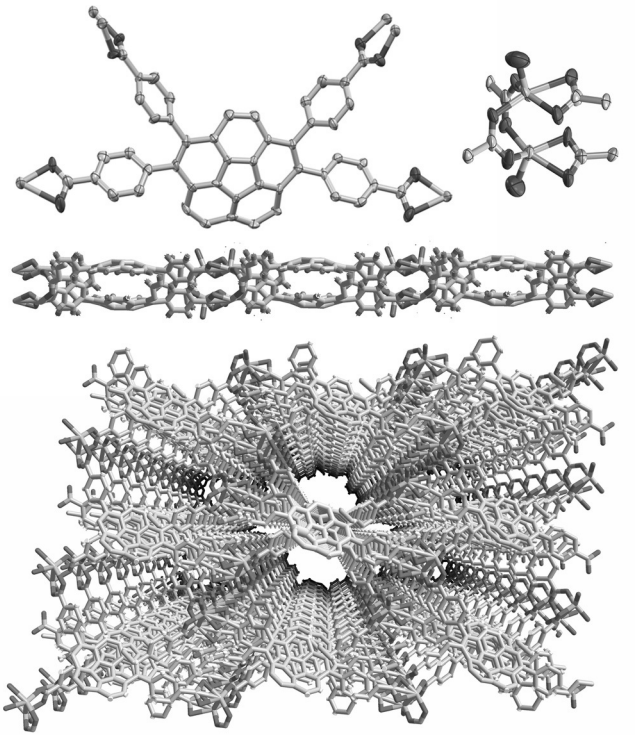

Figure 1. The single-crystal X-ray structure of **1**: DFT^{4-} coordinated to Zn^{2+} (top left) and the $Zn_2(O_2C-)_4$ SBU (top right). Ellipsoids set at 50% probability. Infinite 2D layers parallel to the crystallographic (11-1) plane (middle). Packing of 2D layers forming 1D channels (bottom). Solvent molecules omitted for clarity.

coordination. The ten-step synthetic route employed for the preparation of H_4DFT is shown in Scheme 2. The synthetic details for the preparation of Me_4DFT as a precursor for H_4DFT and its structural elucidation by ^{1}H COSY, $^1H\{^{13}C\}$ HSQC, and $^1H\{^{13}C\}$ HMBC NMR spectroscopy can found in the Supporting Information (Figures S1–S9).[32]

In comparison with naked $C_{20}H_{10}$, decoration of the corannulene core with four electron-withdrawing groups in H_4DFT led to a significantly lowered lowest unoccupied molecular orbital (LUMO) energy level, implying that H_4DFT is a better electron acceptor than unsubstituted $C_{20}H_{10}$ (Figure S10). As shown in Figure S11, H_4DFT has its highest occupied molecular orbital (HOMO) primarily localized on the corannulene bowl. Aside from the corannulene core, significant contributions from two of the benzoic acid groups were observed in the LUMO (Figure S10). The HOMO–LUMO gap of H_4DFT was calculated to be 3.95 eV, which is in line with the acquired spectroscopic data (Figures S12 and S13).

Immobilization of the prepared ligand in a rigid MOF matrix was performed by reacting H_4DFT with $Zn(NO_3)_2$ in a mixture of *N*,*N*-dimethylformamide (DMF) and ethanol, which resulted in the formation of yellow plates of $[Zn_2(DFT)(H_2O)_2(EtOH)]\cdot(H_2O)_{2.85}(DMF)_{0.1}$ (**1**), which were suitable for single-crystal X-ray diffraction analysis.

Crystallographic studies of **1** revealed that coordination of DFT^{4-} to Zn^{2+} led to the formation of a two-dimensional (2D) MOF (Figures 1, S14, and S15; Table S1). Unlike many tetratopic ligands, which typically promote the formation of the common paddlewheel metal nodes,[33–36] the secondary building unit (SBU) in **1** is a strongly distorted ZnO_5 square pyramid. As shown in Figure 1, half of the carboxylates are bonded to two Zn^{2+} ions in a similar motif to that observed in the paddlewheel node, but the other two carboxylates are bonded to one metal ion each, giving rise to a very rare zinc-based SBU. Although the rigid structure of MOFs can significantly affect ligand geometry and, in some cases, lead to highly strained organic linkers,[37] the corannulene molecular conformations in **1** are not flattened or distorted. Figure S16 and Table S2 show a comparison of the DFT^{4-} bowl depth in **1** (0.87 Å)[38] to those in other tetrasubstituted corannulene derivatives,[2,4,39–42] demonstrating that coordinative immobilization has no significant influence on the corannulene bowl curvature. Furthermore, the DFT^{4-} bowl depth in **1** is the same as in parent $C_{20}H_{10}$ (0.87 Å),[38] whereas significant corannulene flattening was previously observed owing to host–guest interactions.[43] The preservation of the undistorted corannulene curvature in DFT^{4-} could perhaps be partially responsible for the significant deviation of the SBU in **1** from the commonly observed paddlewheel metal node. Such preservation of the bowl-shaped DFT^{4-} structure could potentially extend the dimensionality of MOFs and enable the use of corannulene-based linkers as receptors with enclosed cavities for molecular recognition,[44,45] alkali-metal immobilization,[15,46] or selective separation.[47] As shown in Scheme 1 and Figures 1 and S15, the crystal structure of **1** contains an unusual, slightly offset subunit consisting of two DFT^{4-} cupped together, forming a clamshell-like unit along the *b* crystallographic axis. Packing of 2D sheets resulted in the formation of one-dimensional channels oriented along the *a* crystallographic axis with dimensions of 9×13 Å. Evacuated **1** was utilized to determine the permanent porosity, and despite the 2D structure, gas sorption analysis revealed that

1 is permanently porous with a BET surface area of 224(1) $m^2 g^{-1}$ (Figure S17). Aside from single-crystal X-ray and gas sorption analysis, powder X-ray diffraction (PXRD), thermogravimetric analysis, FT-IR spectroscopy, and elemental analysis were employed to study bulk as-synthesized **1** (Figures S18–S23). As shown in Figure S18, the PXRD pattern of **1** coincided with the simulated spectrum from the single-crystal X-ray data.

Owing to a doubly degenerate LUMO, corannulene can accept up to four electrons and has three distinct reduction potentials (Table 1).[48] To test the electrochemical properties

Table 1: Redox potentials of Me_4DFT, H_4DFT, **1**, and $C_{20}H_{10}$.

	E_p(I) [V]	E_p(II) [V]	E_p(III) [V]
Me_4DFT	−1.52	−1.68	−1.94
H_4DFT	−1.64		
1	−1.42	−1.69	
$C_{20}H_{10}$[48]	−1.87	−2.41	−3.13

of synthesized H_4DFT, Me_4DFT, and **1**, cyclic voltammetry measurements were carried out in a DMF solution containing 0.1M tetrabutylammonium hexafluorophosphate, using an H cell equipped with saturated calomel reference, platinum wire counter, and glassy carbon working electrodes. Cyclic voltammetry studies of MOFs are relatively rare and require significant modification of the commonly used electrochemical setup.[49,50] For the electrochemical studies, a small amount of **1** and Nafion were mixed, followed by placement on the surface of the glassy carbon electrode. The cyclic voltammogram (CV) of **1** shows at least two distinct reduction events with peak potentials of $E_p = -1.42$ V and $E_p = -1.69$ V (Figure 2). Similarly, free H_4DFT undergoes one large, irreversible reduction with a peak potential of $E_p = -1.64$ V (Figure 2). The irreversibility and shape of the CV wave for H_4DFT are consistent with the electrochemistry of related benzoic acids.[51] The cyclic voltammogram of Me_4DFT, on the other hand, exhibits three distinct, reversible reductions at $E_{1/2} = -1.52$ V, $E_{1/2} = -1.68$ V, and $E_{1/2} = -1.94$ V (Table 1 and Figure 2). The charges passed and the peak-to-peak separation of about 30 mV (at 20 $mV s^{-1}$ scan rate) of the third redox wave at $E_{1/2} = -1.94$ V indicate that this is a two-electron process. Two-electron redox events are indicative of potential inversion, which is typically associated with significant structural changes occurring during the electron transfer processes.[52] Comparing the simulated and experimental CV data of Me_4DFT provides additional support for the two-electron reduction assignment (Figure 2). Comparison of the acquired CV data with that of corannulene shows that each reduction potential of Me_4DFT is markedly less negative;[48] $E_{1/2}$(I), $E_{1/2}$(II), and $E_{1/2}$(III) are less negative by +0.35 V, +0.73 V, and +0.62 V, respectively (Table 1). Similarly, the reduction potentials for **1** are also less negative, with values of $\Delta E_{1/2}(I) = +0.45$ V and $\Delta E_{1/2}(II) = +0.72$ V compared to unmodified $C_{20}H_{10}$. Thus, cyclic voltammetry confirmed the stronger electron-accepting ability of the prepared compounds versus naked $C_{20}H_{10}$.

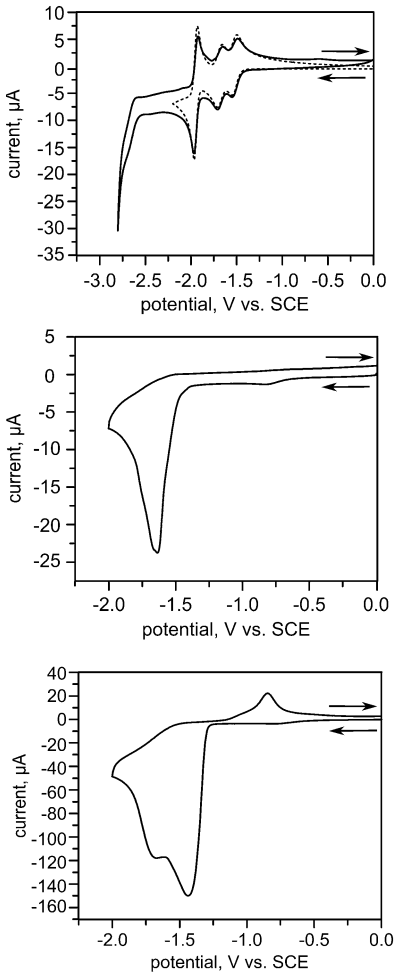

Figure 2. Cyclic voltammograms of Me_4DFT (top, ——), simulated (top, •••••), H_4DFT (middle), and **1** (bottom). The reduction potentials for the four reversible reductions, $Me_4DFT + e^- \rightleftharpoons [Me_4DFT]^-$, $[Me_4DFT]^- + e^- \rightleftharpoons [Me_4DFT]^{2-}$, $[Me_4DFT]^{2-} + e^- \rightleftharpoons [Me_4DFT]^{3-}$, and $[Me_4DFT]^{3-} + e^- \rightleftharpoons [Me_4DFT]^{4-}$, were set to E(I) = −1.52 V, E(II) = −1.68 V, E(III) = −2.05 V, and E(IV) = −1.80 V.

As H_4DFT, Me_4DFT, and **1** exhibit bright emission detectable by the naked eye, their photophysical properties were investigated by fluorescence, UV/Vis, and diffuse-reflectance spectroscopy (Figure 3). The emission maximum of Me_4DFT was located at 443 nm (Figure S24). The photoluminescence maxima of solid H_4DFT ($\lambda_{max} = 470$ nm, Figure S13) and **1** ($\lambda_{max} = 472$ nm, Figure 3) exhibit a bathochromic shift by about 20 nm, in comparison with solid unsubstituted $C_{20}H_{10}$, which could be explained in part by the attachment of electron-withdrawing groups to the corannulene core and the extended π system of the tetrasubstituted linker.[53,54] Interestingly, the measured fluorescence quantum yields (Φ) of H_4DFT and Me_4DFT in solution are more than twice as large as those of the unsubstituted corannulene.[54] Moreover, the Φ value of H_4DFT in the solid state is comparable to the value acquired in solution, and therefore, prepared H_4DFT does not suffer from aggregation-caused quenching, which is a common phenomenon for chromophores in the solid state.[55,56] Both in solution and in the solid state, H_4DFT possesses the highest fluorescence quantum

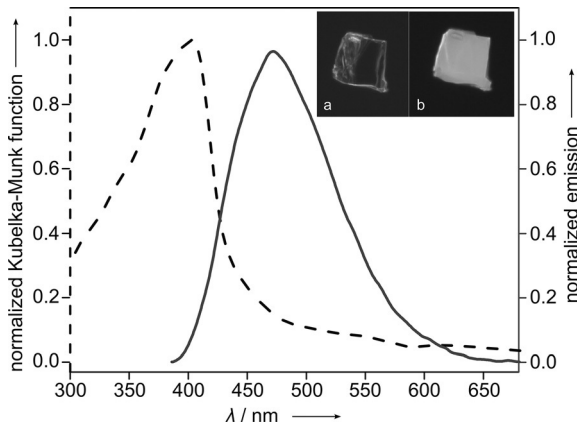

Figure 3. Normalized diffuse reflectance (– – –) and emission (——) spectra of **1**. The inset shows epifluorescence microscopy images of a crystal of **1** before (a) and after (b) irradiation at $\lambda_{ex} = 370$ nm.

yield among these compounds, and Φ_{solid} is comparable with that of **1** (Table 2).

Table 2: Photophysical properties of Me_4DFT, H_4DFT, **1**, and $C_{20}H_{10}$.

	Me_4DFT	H_4DFT	**1**	$C_{20}H_{10}$
$\Phi_{solution}$[b] [%]	17.54 ± 0.29	18.62 ± 0.08	–	7.0 ± 0.1[a]
Φ_{solid} [%]	6.37 ± 0.03	12.50 ± 0.60	11.45 ± 0.60	–
$\lambda_{em,\,max}$[c] [nm]	450	470	472	454[a]

[a] The values were obtained from Refs. [53] and [54]. [b] Measurements conducted in THF. [c] Photoluminescence measurements performed in the solid state.

In conclusion, we have developed the first example of a porous crystalline hybrid scaffold in which redox-active corannulene-based ligands are covalently coordinated to metal ions. The ten-step synthesis of the corannulene-containing linker, which is thus available on a gram scale and necessary for the scaffold preparation, has also been reported. Comprehensive analysis of the new corannulene-based compounds demonstrates their better electron-accepting properties in comparison with unmodified corannulene. Moreover, the photoluminescence quantum yields of the prepared derivatives are almost double that of naked $C_{20}H_{10}$. Single-crystal X-ray analysis revealed the preservation of the corannulene bowl after coordinative immobilization inside the rigid scaffold, which offers an extension of MOF dimensionality through the corannulene curvature. The preliminary results demonstrate that the doping of **1** with these donor molecules results in a charge-transfer band. Further work in this direction is in progress. The presented work constitutes the first attempt to merge the modularity and porosity inherent to MOFs with the intrinsic properties of π-bowls, which could open a new avenue for the rational design of electroactive multidimensional crystalline porous materials.

Experimental Section

Full experimental details data can be found in the Supporting Information. CCDC 1429960 (**1**) contains the supplementary crystallographic data for this paper. These data can be obtained free of charge from The Cambridge Crystallographic Data Centre.

Acknowledgements

This work was partially supported by ASPIRE-I and III awards granted by the USC Office of the Vice President for Research. Crystallographic data were collected through the Service Crystallography at Advanced Light Source Program at beamline 11.3.1 at the Advanced Light Source (ALS), Lawrence Berkeley National Laboratory. The ALS is supported by the U.S. Department of Energy, Office of Basic Energy Sciences, Materials Sciences Division (DE-AC02-05CH11231).

Keywords: coordination polymers · corannulene · cyclic voltammetry · fluorescence · metal–organic frameworks

How to cite: *Angew. Chem. Int. Ed.* **2016**, *55*, 2195–2199
Angew. Chem. **2016**, *128*, 2235–2239

[1] W. E. Barth, R. G. Lawton, *J. Am. Chem. Soc.* **1966**, *88*, 380–381.
[2] Y. Wu, D. Bandera, R. Maag, A. Linden, K. K. Baldridge, J. S. Siegel, *J. Am. Chem. Soc.* **2008**, *130*, 10729–10739.
[3] Y. Wu, J. S. Siegel, *Chem. Rev.* **2006**, *106*, 4843–4867.
[4] B. Topolinski, B. M. Schmidt, S. Schwagerus, M. Kathan, D. Lentz, *Eur. J. Inorg. Chem.* **2014**, 5391–5405.
[5] C. Dubceac, A. S. Filatov, A. V. Zabula, A. Y. Rogachev, M. A. Petrukhina, *Chem. Eur. J.* **2015**, *21*, 14268–14279.
[6] R. Warmbier, A. Quandt, G. Seifert, *J. Phys. Chem. C* **2014**, *118*, 11799–11805.
[7] A. M. Butterfield, B. Gilomen, J. S. Siegel, *Org. Process Res. Dev.* **2012**, *16*, 664–676.
[8] A. Sygula, F. R. Fronczek, R. Sygula, P. W. Rabideau, M. M. Olmstead, *J. Am. Chem. Soc.* **2007**, *129*, 3842–3843.
[9] L. Zoppi, L. Martin-Samos, K. K. Baldridge, *J. Am. Chem. Soc.* **2011**, *133*, 14002–14009.
[10] G. Valenti, C. Bruno, S. Rapino, A. Fiorani, E. A. Jackson, L. T. Scott, F. Paolucci, M. Marcaccio, *J. Phys. Chem. C* **2010**, *114*, 19467–19472.
[11] J. Mack, P. Vogel, D. Jones, N. Kaval, A. Sutton, *Org. Biomol. Chem.* **2007**, *5*, 2448–2452.
[12] L. Kobryn, W. P. Henry, F. R. Fronczek, R. Sygula, A. Sygula, *Tetrahedron Lett.* **2009**, *50*, 7124–7127.
[13] G. Sandí, R. E. Gerald, L. G. Scanlon, C. S. Johnson, R. J. Klingler, J. W. Rathke, *J. New Mater. Electrochem. Syst.* **2000**, *3*, 13–19.
[14] H. Yokoi, Y. Hiraoka, S. Hiroto, D. Sakamaki, S. Seki, H. Shinokubo, *Nat. Commun.* **2015**, *6*, 8215.
[15] A. V. Zabula, A. Y. Rogachev, M. A. Petrukhina, *Science* **2011**, *333*, 1008–1011.
[16] Q. Xie, E. Perez-Cordero, L. Echegoyen, *J. Am. Chem. Soc.* **1992**, *114*, 3978–3980.
[17] I. V. Kuvychko, S. N. Spisak, Y.-S. Chen, A. A. Popov, M. A. Petrukhina, S. H. Strauss, O. V. Boltalina, *Angew. Chem. Int. Ed.* **2012**, *51*, 4939–4492; *Angew. Chem.* **2012**, *124*, 5023–5026.
[18] R. E. Gerald, R. J. Klingler, G. Sandí, C. S. Johnson, L. G. Scanlon, J. W. Rathke, *J. Power Sources* **2000**, *89*, 237–243.
[19] R. Lu, W. Xuan, Y. Zheng, Y. Zhou, X. Yan, J. Dou, R. Chen, J. Pei, W. Weng, X. Cao, *RSC Adv.* **2014**, *4*, 56749–56755.

[20] M. C. Stuparu, *Angew. Chem. Int. Ed.* **2013**, *52*, 7786 – 7790; *Angew. Chem.* **2013**, *125*, 7940 – 7944.
[21] E. L. Elliott, G. A. Hernández, A. Linden, J. S. Siegel, *Org. Biomol. Chem.* **2005**, *3*, 407 – 413.
[22] Y. Sevryugina, E. A. Jackson, L. T. Scott, M. A. Petrukhina, *Inorg. Chim. Acta* **2008**, *361*, 3103 – 3108.
[23] S. N. Spisak, A. V. Zabula, A. S. Filatov, M. A. Petrukhina, *J. Organomet. Chem.* **2015**, *784*, 69 – 74.
[24] A. Ayalon, A. Sygula, P. C. Cheng, M. Rabinovitz, P. W. Rabideau, L. T. Scott, *Science* **1994**, *265*, 1065 – 1067.
[25] F. Furrer, A. Linden, M. C. Stuparu, *Chem. Eur. J.* **2013**, *19*, 13199 – 13206.
[26] S. Ito, Y. Tokimaru, K. Nozaki, *Angew. Chem. Int. Ed.* **2015**, *54*, 7256 – 7260; *Angew. Chem.* **2015**, *127*, 7364 – 7368.
[27] S. Da Ros, A. Linden, K. K. Baldridge, J. S. Siegel, *Org. Chem. Front.* **2015**, *2*, 626 – 633.
[28] K. K. Tanabe, S. M. Cohen, *Chem. Soc. Rev.* **2011**, *40*, 498 – 519.
[29] J. Lee, O. K. Farha, J. Roberts, K. A. Scheidt, S. T. Nguyen, J. T. Hupp, *Chem. Soc. Rev.* **2009**, *38*, 1450 – 1459.
[30] D. F. Sava Gallis, L. E. S. Rohwer, M. A. Rodriguez, T. M. Nenoff, *Chem. Mater.* **2014**, *26*, 2943 – 2951.
[31] K. Lu, C. He, W. Lin, *J. Am. Chem. Soc.* **2014**, *136*, 16712 – 16715.
[32] D. Pappo, T. Mejuch, O. Reany, E. Solel, M. Gurram, E. Keinan, *Org. Lett.* **2009**, *11*, 1063 – 1066.
[33] J. L. C. Rowsell, O. M. Yaghi, *Microporous Mesoporous Mater.* **2004**, *73*, 3 – 14.
[34] N. B. Shustova, B. D. McCarthy, M. Dincă, *J. Am. Chem. Soc.* **2011**, *133*, 20126 – 20129.
[35] B. Q. Ma, K. L. Mulfort, J. T. Hupp, *Inorg. Chem.* **2005**, *44*, 4912 – 4914.
[36] T. A. Makal, W. Zhuang, H.-C. Zhou, *J. Mater. Chem. A* **2013**, *1*, 13502 – 13509.
[37] N. B. Shustova, A. F. Cozzolino, M. Dincă, *J. Am. Chem. Soc.* **2012**, *134*, 19596 – 19599.
[38] J. C. Hanson, C. E. Nordman, *Acta Crystallogr. Sect. B* **1976**, *32*, 1147 – 1153.
[39] A. S. Filatov, A. K. Greene, E. A. Jackson, L. T. Scott, M. A. Petrukhina, *J. Organomet. Chem.* **2011**, *696*, 2877 – 2881.
[40] R. Maag, B. H. Northrop, A. Butterfield, A. Linden, O. Zerbe, Y. M. Lee, K.-W. Chi, P. J. Stang, J. S. Siegel, *Org. Biomol. Chem.* **2009**, *7*, 4881 – 4885.
[41] B. D. Steinberg, E. A. Jackson, A. S. Filatov, A. Wakamiya, M. A. Petrukhina, L. T. Scott, *J. Am. Chem. Soc.* **2009**, *131*, 10537 – 10545.
[42] H. B. Lee, P. R. Sharp, *Organometallics* **2005**, *24*, 4875 – 4877.
[43] M. Juríček, N. L. Strutt, J. C. Barnes, A. M. Butterfield, E. J. Dale, K. K. Baldridge, J. F. Stoddart, J. S. Siegel, *Nat. Chem.* **2014**, *6*, 222 – 228.
[44] D. Moon, S. Kang, J. Park, K. Lee, R. P. John, H. Won, G. H. Seong, Y. S. Kim, G. H. Kim, H. Rhee, M. S. Lah, *J. Am. Chem. Soc.* **2006**, *128*, 3530 – 3531.
[45] M. M. Conn, J. Rebek, *Chem. Rev.* **1997**, *97*, 1647 – 1668.
[46] A. S. Filatov, A. V. Zabula, S. N. Spisak, A. Y. Rogachev, M. A. Petrukhina, *Angew. Chem. Int. Ed.* **2014**, *53*, 140 – 145; *Angew. Chem.* **2014**, *126*, 144 – 149.
[47] R. Warmuth, J. Yoon, *Acc. Chem. Res.* **2001**, *34*, 95 – 105.
[48] C. Bruno, R. Benassi, A. Passalacqua, F. Paolucci, C. Fontanesi, M. Marcaccio, E. A. Jackson, L. T. Scott, *J. Phys. Chem. B* **2009**, *113*, 1954 – 1962.
[49] X. Wang, J. Zhou, H. Fu, W. Li, X. Fan, G. Xin, J. Zheng, X. Li, *J. Mater. Chem. A* **2014**, *2*, 14064 – 14070.
[50] C. R. Wade, M. Li, M. Dincă, *Angew. Chem. Int. Ed.* **2013**, *52*, 13377 – 13381; *Angew. Chem.* **2013**, *125*, 13619 – 13623.
[51] B. D. McCarthy, D. J. Martin, E. S. Rountree, A. C. Ullman, J. L. Dempsey, *Inorg. Chem.* **2014**, *53*, 8350 – 8361.
[52] D. H. Macías-Ruvalcaba, N. A. Evans, *J. Phys. Chem. B* **2005**, *109*, 14642 – 14647.
[53] J. Dey, A. Y. Will, R. A. Agbaria, P. W. Rabideau, A. H. Abdourazak, R. Sygula, I. M. Warner, *J. Fluoresc.* **1997**, *7*, 231 – 236.
[54] A. S. Filatov, E. A. Jackson, L. T. Scott, M. A. Petrukhina, *Angew. Chem. Int. Ed.* **2009**, *48*, 8473 – 8476; *Angew. Chem.* **2009**, *121*, 8625 – 8628.
[55] Y. Hong, J. W. Y. Lam, B. Z. Tang, *Chem. Soc. Rev.* **2011**, *40*, 5361 – 5388.
[56] J. Luo, Z. Xie, J. W. Lam, L. Cheng, H. Chen, C. Qiu, H. S. Kwok, X. Zhan, Y. Liu, D. Zhu, B. Z. Tang, *Chem. Commun.* **2001**, 1740 – 1741.

Received: October 12, 2015
Revised: December 2, 2015
Published online: December 22, 2015

